PAPER

Check for updates

In situ preparation of C–SiCxOy coatings with controllable composition on continuous oxygen-enriched SiC fibres

Haonan Xu, [ID] [ab] Qi Wang, [ab] Hongrui Xiao, [ab] Xiangdong Li, [ab] Xiaohui Su, [ab] Ming Tang, [ab] Lifu Chen [ab] and Siwei Li*[ab]

Oxygen-enriched SiC fibres derived from polycarbosilane are exposed to chlorine at 500 to 750 °C for up to 60 min. After chlorination, uniform coatings with controllable thickness are formed *in situ* on the SiC fibres. Evolution of the coating composition and its relation to the electrical properties are investigated. Results indicate that the porous nature of the coating realizes a reaction-controlling mechanism of the coating growth. By enhancing the chlorination temperature within the selected range, SiC, $SiCO_3$ and SiC_2O_2 phases in the fibre can be successively etched as free carbon to give C–SiCxOy hybrid coatings with increased content of C and decreased content of O. Accordingly, the specific resistivity of the coated SiC fibre declines continuously from 5.01×10^6 to 0.39 Ω cm.

1 Introduction

With the advantages of thermal stability, low density, high strength and excellent oxidation resistance,[1–3] polymer derived SiC-based fibres are widely used for fabricating thermal structural composites with specific aims. Nowadays, the most important application of SiC-based fibres is to toughen ceramics through mechanisms of interfacial debonding and microcrack deflecting.[4–6] In this case, fibre layers are required to generate controllable weak bonding between the SiC fibre and the ceramic matrix.[7,8] For the SiC-based fibres, the most popular species of surface layers are known as pyrolytic carbon (PyC) and boron nitride (BN),[9–11] which are commonly prepared by a costly approach of chemical vapor infiltration (CVI). Y. G. Gogotsi. *et al.* developed a less expensive method to prepare carbide-derived carbon (CDC) coatings on SiC fibres by using hydrothermal treatment or halogen etching.[12] Uniform carbon coatings are obtained with a good adherence to the SiC fibres. Mechanical properties of the SiC fibres are even improved after formation of the carbon coating with optimized thickness[13] Moreover, thanks to the porous nature, the CDC layers can also be used as templates for yielding BN coatings *via* inexpensive chemical routes.[14–17]

A. Delcamp *et al.* reported the kinetics of the growth of the CDC coating on two types of the SiC-based fibres, Tyranno ZMI and Nicalon.[18] In the temperature range of 550–675 °C, the

coating thickness is found to increase linearly with the etching time (in Cl_2 environment), suggesting that the coating growth is controlled by interfacial reaction. It should be noted that oxygen of ∼9 at% and ∼14 at% is present in the Tyranno ZMI and Nicalon fibre, respectively. But compositions of the resultant CDC coatings on both fibres are all considered as pure carbon. Assisted by thermodynamic calculation, the authors suggested that oxygen impurities would be extracted as gases during chlorination by reacting with residual carbon then with Cl_2. However, the equilibrium results may not represent the real case as they do not account for the kinetics of the process. Also, the calculations could not be responsible for the evolution of the metaphases, which may influence the composition and function of the SiC fibre to a great extent. We recently found that if an oxygen-enriched SiC fibre (oxygen content is comparable to Nicalon fibre) was exposed to Cl_2 at above 500 °C, the oxygen content in the resultant CDC coating decreased gradually with elevated temperatures. This suggests that the tetrahedral metaphases of SiCxOy (SiC_3O, SiC_2O_2, $SiCO_3$) in the SiC fibre can be selectively etched into free carbon. Therefore, the coating formed at the fibre surface is not pure carbon but actually C–SiCxOy hybrid phases with variable C/SiCxOy ratios. Change of the coating composition offers great possibilities for modifying the behaviour of interfacial debonding and fibre pullout, and may also endow the composites new functions, such as controllable resistivity and dielectric performance. Moreover, the doping of SiCxOy in the fibre coating may enhance the oxidation resistance of the fibre as compared with the pure carbon coatings. The current work focuses on the influence of chlorination on microstructure of the C–SiCxOy hybrid coatings. Controllability of the electrical resistivity of the coating by the chlorination is also discussed.

[a]College of Materials, Key Laboratory of High Performance Ceramic Fibers, Xiamen University, Xiamen 361005, China. E-mail: swli@xmu.edu.cn

[b]Fujian Key Laboratory of Advanced Materials, Key Laboratory of High Performance Ceramic Fibers of Ministry of Education, College of Materials, Xiamen University, Xiamen 361005, China

Table 1 Weight loss and coating thickness of the treated SiC fibres

Sample	Temperature (°C)	Soaking time (min)	Weight loss (wt%)	Coating thickness (μm)
500-5	500	5	0.80	Invisible in SEM
500-30	500	30	3.30	0.141 ± 0.015
500-60	500	60	5.54	0.326 ± 0.013
550-5	550	5	7.82	0.426 ± 0.017
550-30	550	30	19.46	1.016 ± 0.027
550-60	550	60	38.82	1.603 ± 0.015
600-5	600	5	18.01	0.591 ± 0.017
600-30	600	30	70.79	1.954 ± 0.093
600-60	600	60	80.49	Go through the fibre
650-5	650	5	40.55	1.285 ± 0.039
700-5	700	5	72.99	4.382 ± 0.045
750-5	750	5	78.77	Go through the fibre

2   Materials preparation

2.1   Preparation of the oxygen-enriched SiC fibre

The oxygen-enriched SiC fibre is prepared following Yajima's route.[1] Polycarbosilane (PCS) with an average molecular weight (M) of 1230 and softening point of 198 °C is used as the precursor. Continuous SiC fibres with a Si/C/O mass ratio of 54/30/16 are obtainable after the processes of melt-spinning, oxidation curing and pyrolysis.

2.2   Chlorination of the SiC fibre

The as-pyrolyzed SiC fibres were placed in a graphite boat and then put into a horizontal quartz tube furnace with inner tube diameter of 30 mm. The fibres were first treated in high purity N_2 (99.999%, 100 ml min^{-1}) from room temperature to 500 °C, the N_2 was cut down and the Cl_2 gas (99.999%, 60 ml min^{-1}) was blown into the furnace tube in the temperature range of 500–750 °C, holding for 5–60 minutes. After the chlorination, the Cl_2 was immediately diluted by the N_2, and the furnace was cooled down in the N_2. An NaOH solution with a concentration of 30 mol% was used to capture the reaction products of $SiCl_4$ and residual Cl_2 gas.

2.3   Characterization

Scanning electron microscopy (SEM, SU70, Hitachi, Japan) was used to observe the fracture morphology and the coating thickness. Transmission electron microscopy (TEM, JEM2100, JEOL, Japan) was used to observe the microstructure of the fibre. X-ray diffraction (XRD; Bruker-AXS, USA) was used for phase identification. Auger electron spectroscopy (AES; PHI660, USA) with an electron beam of 5 keV (100 nA) was used for analysing the coating composition. The sputtering rate was estimated to be 11 nm min^{-1} (for SiO_2). X-ray photoelectron spectroscopy (XPS; PHI Quantum 2000, USA) analysis was carried out to give chemical states by employing $AlK_{\alpha1,2}$ radiation of 1486.60 eV. Resistance (R) of SiC fibre was measured using the two-points testing method.[19] Specific resistivity (ρ) was calculated by the formula $\rho = RS/L$.

The pull-out tests were conducted on $SiC_f/SiOC$ composites. The as-received SiC fibres coated with C–SiC_xO_y coatings were used as the reinforcement for this study. Commercial available poly-methylsilsesquioxane (MK resin, Wacker-Chemie GmbH, München, Germany), with relative molecular mass 9100 g mol^{-1} and softening point 35–55 °C, was used as the precursor to SiOC glasses. The composites were fabricated by precursor infiltration and pyrolysis (PIP) process.

3   Results and discussion

3.1   Effect of chlorination on the microstructure of the C–SiC_xO_y hybrid coating

A series of samples are obtained by controlling the chlorination temperature and soaking time. Weight loss and coating thickness of the treated SiC fibres are shown in Table 1. It can be seen that the deviations of the coating thickness measured for all treatments are quite small, indicating a homogeneous infiltration of Cl_2 with within fibre tows during reaction. The coating thickness evidently increases with the increase in temperature and prolonged soaking time. After chlorination at 500 °C for 5 minutes, the weight loss is identified as 0.8 wt%, revealing that the Cl_2 starts to react with the fibre. At this time, the resultant coating is too thin to be observed in SEM (see Fig. 1). After chlorination at 600 °C for 5 min, the coating grows intensively to an average thickness of 591 nm. In case of treating at 750 °C for 5 minutes, the chlorination goes through the whole fibre, thus the interface of the fibre/coating disappears.

Fig. 2a shows the change of fibre weight and coating thickness as function of chlorination temperature. The loss of the fibre weight has a trend similar to the growth of the fibre coating. For both curves, a rapid enhancement is observed at above 600 °C, indicating that the chlorination is accelerated at this point. It is worth noting that weight loss of the 750-5 sample and the 600-60 sample reach 79 wt% and 80 wt% respectively. Both values are much higher than the Si content (54 wt%) of the as-prepared SiC fibre, indicating that more elements in addition to Si are extracted from fibre. It is thus concluded that the presence of the SiC_xO_y phases lead to removal of C and O in the Cl_2 environment. The possible reactions are as follows.[20,21]
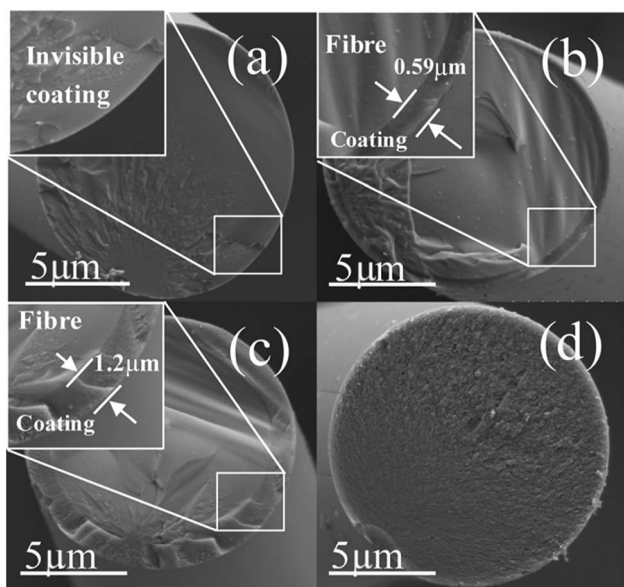
Fig. 1 Cross-section morphology of the fibres before and after chlorination. (a) The as-pyrolyzed SiC fibre, (b) 600-5, (c) 650-5, (d) 750-5.

$$SiC(s) + 2Cl_2(g) = C(s) + SiCl_4(g) \qquad (1)$$

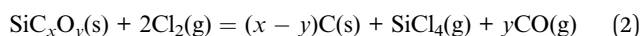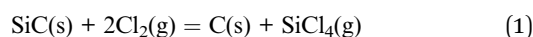$$SiC_xO_y(s) + 2Cl_2(g) = (x - y)C(s) + SiCl_4(g) + yCO(g) \qquad (2)$$

Fig. 2b shows the influence of isothermal process on the fibre weight and the coating thickness. The thickness increases almost linearly with the soaking time, suggesting that the kinetics of coating growth is controlled by interfacial reaction rather than diffusion of the Cl_2.

The porous structure of CDC coating is characterized using low-temperature nitrogen sorption method. The isotherm curve of nitrogen adsorption displayed in Fig. 3a presents an increasing uptake at relative pressure between 0.05 and 0.3 (a type I form according to IUPAC classification),[22] indicating the existence of micropores in the CDC coating. Specific surface area (SSA) is calculated using the BET equation (Fig. 3b). The SSA of the coating increases with elevating temperature, which is in accordance with the results in ref. 18. However, since the thickness of the CDC coatings obtained at various temperatures is different, the true weight percentage of the porous region (CDC coating in the fibre) is changeable and unmeasurable for different samples. This will introduce errors to the BET calculation. Taking this into account, different fibres (600-60 and 750-5) with whole body of CDC are used to determine the BET characters to eliminate the influence of coating thickness. The SSA of the 750-5 is identified to be much higher than that of the 600-60, while the average pore width of the former (1.56 nm) is close to that of the latter (1.62 nm). It is obvious that more phases in the SiC fibre are consumed as gases at higher temperatures. As a result, more micropores are generated to enhance the SSA. According to the BET results, there should be evident differences in the reactivity of Cl_2 with different phases in the SiC fibre.

Surface composition of the fibre coating is examined by AES. After chlorination, the Si peaks at fibre surface are significantly weakened whereas the C peaks are intensified (Fig. 4a), proving that Si atoms are diminished from the fibre. The chlorination is found to proceed evenly as the growth of the coating since the elements distribute uniformly along the thickness direction, as shown in the depth-profile of 550-5 sample (Fig. 4b). It is also seen form Fig. 4b that the O content of the coating is very close to that of the fibre core, revealing that the oxygen containing phases in the fibre are relatively more stable than the SiC domains. The Si and C gradients of 200 nm observed between coating and fibre are most likely induced by dilution of Cl_2 and reduction of reactivity as it moves inward the fibre during the cooling process. Fig. 5 shows variations of the coating composition with chlorination temperature and soaking time. At elevated temperatures, the content of Si and O gradually decreased while the content of C correspondingly increased. Nevertheless, the isothermal process has little impact on the elemental concentration. Combining Fig. 2b, it is evident that reaction temperature is the key factor to control the coating composition, while changing the soaking time is mainly related to variation of the coating thickness. To meet different
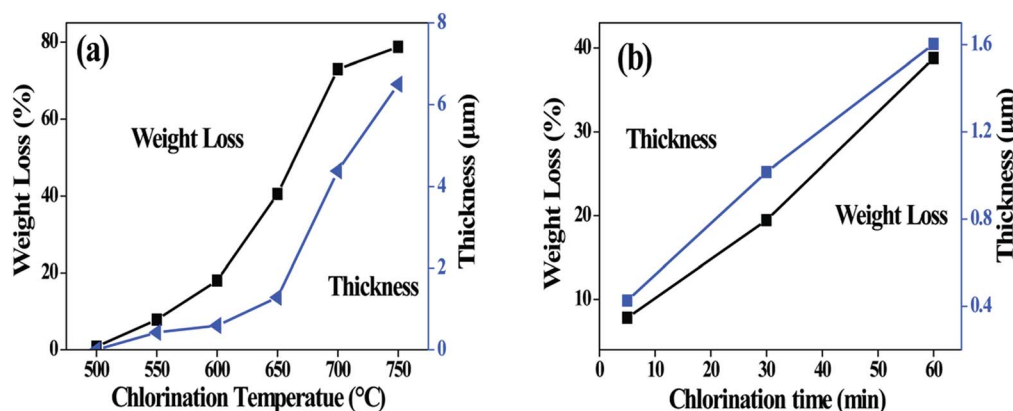

Fig. 2 Change in fibre weight and coating thickness with (a) chlorination temperature and (b) soaking time. The holding time for (a) is 5 min, and the chlorination temperature for (b) is 550 °C.
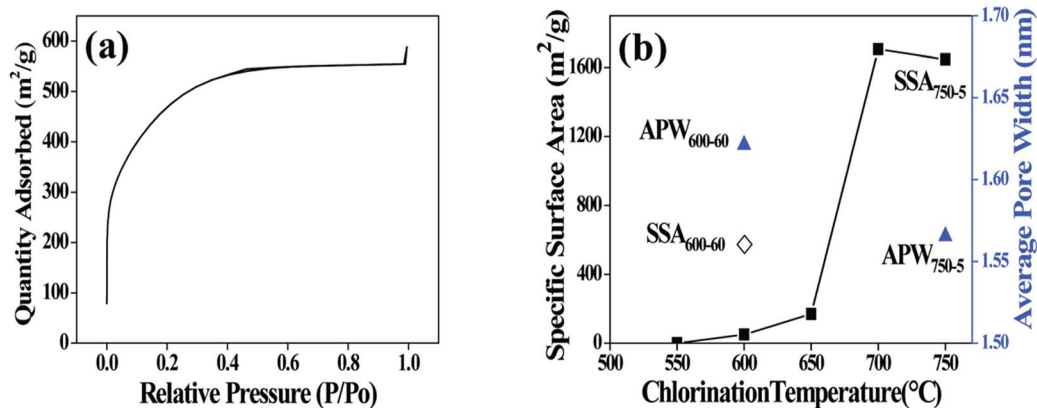
Fig. 3 (a) N_2 adsorption and desorption isotherm linear plot of 700-5 sample. (b) Calculated specific surface area (SSA) and average pore width (APW) of the chlorinated fibres. ($\diamondsuit$) represents SSA of 600-60. ($\blacksquare$) represent SSA of the fibre chlorinated at different temperatures for 5 min. ($\blacktriangle$) represent PW of 600-60 and 750-5.
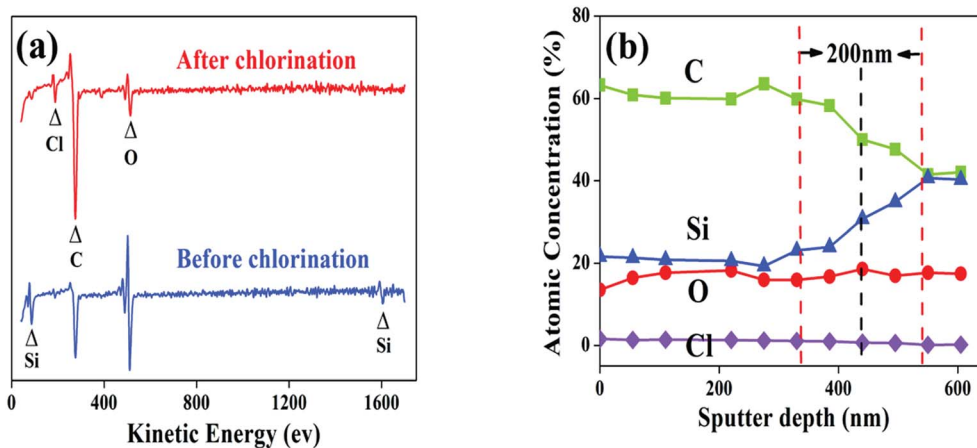

Fig. 4 (a) AES spectra on the surface of as-pyrolyzed SiC fibre and 700-5 sample. (b) AES depth-profile of the 550-5 sample.

purposes, the composition and thickness of the coating can be independently regulated.

The chemical state of the fibre coatings is characterized by XPS. Fig. 6 illustrates the spectra of Si 2p, C 1s, O 1s and the fitted results. Based on the structural characters of the PCS-SiC fibres, the Si peak is fitted into the following five sub-peaks: SiC_4 (refers to SiC phase), SiC_3O, SiC_2O_2, $SiCO_3$ and SiO_4 (refers to SiO_2 phase) with binding energies of 100.7, 101.6, 102.6, 103.4 and 104.3 eV respectively.[23-25] Accordingly, the C spectra are fitted into four peaks of C–Si, C–C, C–O and C=O (refers to
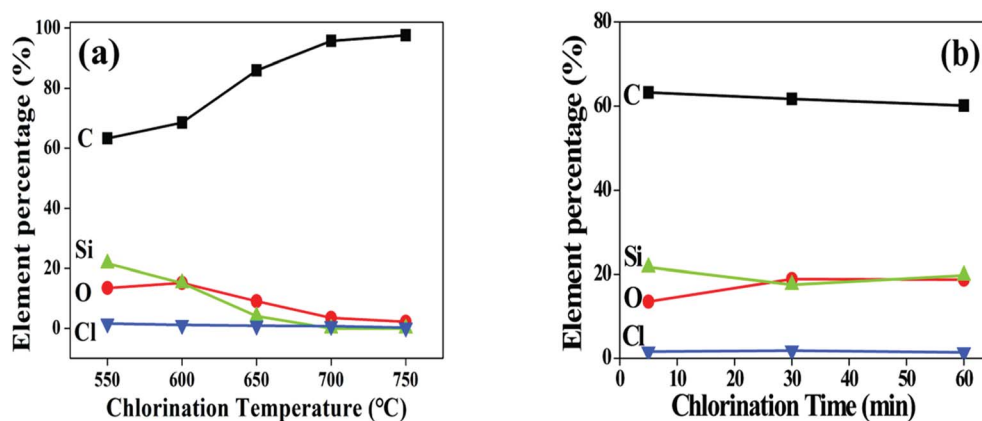

Fig. 5 Variations of coating composition as function of chlorination temperature and soaking time. (a) Chlorination for 5 min with temperature range from 550 to 750 °C. (b) Chlorination at 550 °C for 5 to 60 minutes.
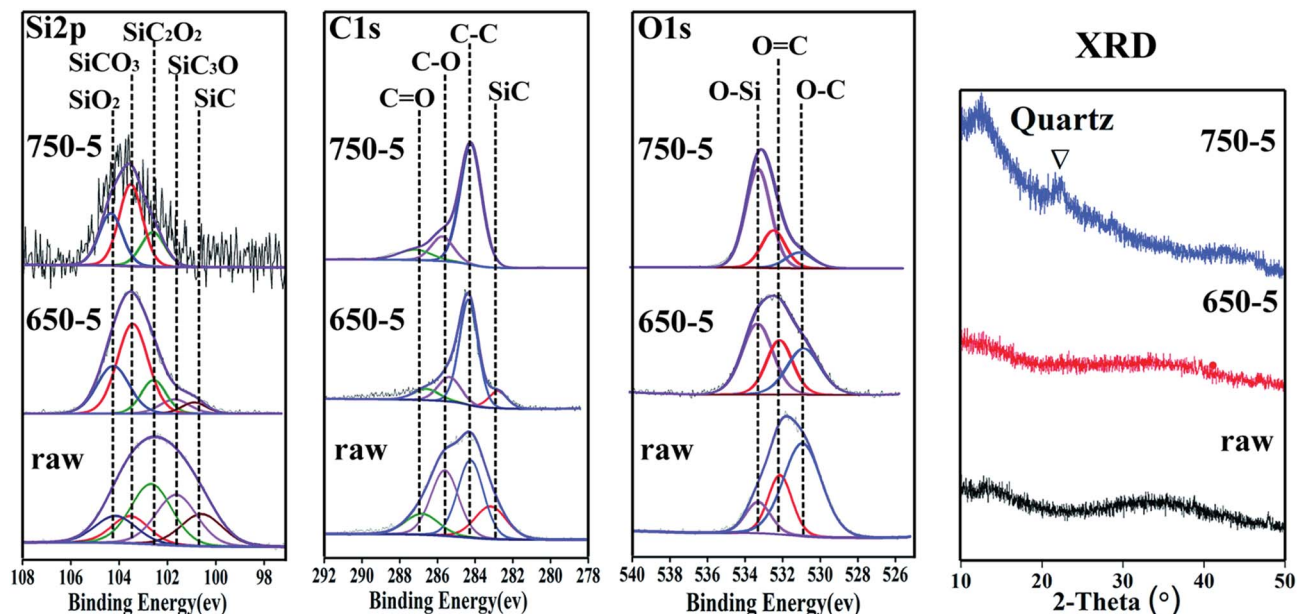
Fig. 6 The fitted XPS spectra of Si 2p, C 1s, O 1s and the related XRD pattern.

Table 2 Relative content (mole fraction) of the phases calculated by the XPS fitted results

	Si (mol%)					O (mol%)			C (mol%)			
	SiC	SiC$_3$O	SiC$_2$O$_2$	SiCO$_3$	SiO$_2$	O–Si	O=C	O–C	C–Si	C–C	C–O	C=O
Raw	16.7	25.9	30.9	12.6	13.9	18.3	18.6	63.1	18.4	36.1	32.9	12.6
500-5	10.7	16.4	30.5	24.1	18.3	20.1	21.3	58.6	17.4	38.8	31.3	12.5
550-5	10.4	15.4	24.4	28	21.8	28.3	20.4	51.3	17.3	40.3	27.7	14.7
600-5	7.4	9.3	24.1	31	28.2	40.6	21.8	37.6	12.9	58.8	21.2	7.1
650-5	4.8	7.1	14.3	47.6	26.2	44.6	25.3	30.1	10.2	63.7	16.2	9.9
750-5	0	0	21.2	48.1	30.7	51.5	24.7	23.8	0	74.6	13.6	11.8

residual gas product of CO) with binding energies of 283.0, 284.5, 285.8 and 287.0 eV respectively.[26,27] The O spectra is fitted as three peaks of O–C, O=C and O–Si with binding energies of 531.2, 532.1 and 533.4 eV, respectively.[28–30] The relative content of the tetrahedral phases is calculated based on the fitted results, as listed in Table 2. With increasing temperature, the relative contents of SiC and SiC$_3$O decreased evidently. Also, SiC$_2$O$_2$ is lowered in concentration but in a slower speed. It is obvious that the Cl$_2$ reacts with SiC and SiC$_3$O much more intense than with SiC$_2$O$_2$. Considering that the bonding energy of Si–Cl is smaller than Si–O but larger than SiC, the erosiveness of Cl$_2$ to SiC$_x$O$_y$ should decline significantly as the increase of the O/Si (y/x) ratio. This is verified by the fact that relative content of the SiO$_2$ and SiCO$_3$ in the coating increased with the elevated chlorination temperature. The XRD graphs also detect the residue of SiO$_2$, wherein a broad peak corresponding to amorphous SiO$_2$ appears in 750-5 sample.

To further evidence the microstructural evolution, TEM observation is conducted and shown in Fig. 7. The as-pyrolyzed SiC fibre shows dense (Fig. 7a) and amorphous structure doped by nano-sized SiC grains (Fig. 7b). Although the chlorinated
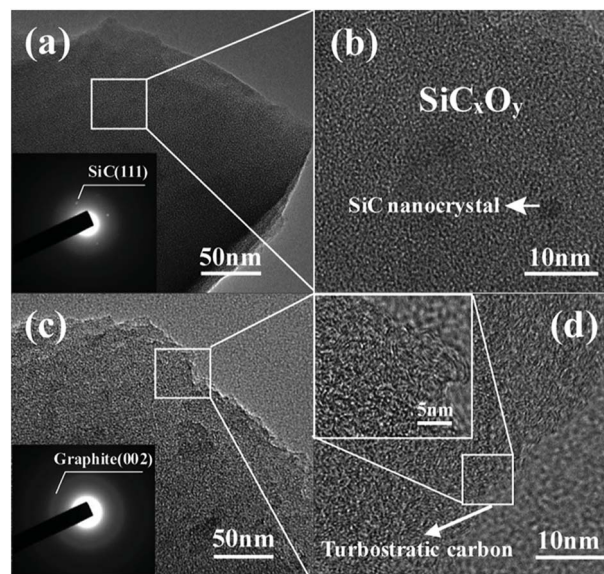

Fig. 7 TEM observations on the fibre before and after chlorination. (a) Low and (b) high magnification image of as-pyrolyzed fibre. (c) Low and (d) high magnification image of 750-5 sample.

Table 3 Electric resistivity of coated SiC fibres and the surface coatings (Ω cm)[a]

	500 °C	550 °C	600 °C	650 °C	700 °C	750 °C
5 min	4.81×10^6 (NA)	5.0×10^4 (5.9×10^3)	83.91 (13.57)	7.8 (2.60)	1.34 (1.15)	0.39 (0.39)
30 min	3.01×10^6 (1.2×10^5)	2.03×10^4 (5.5×10^3)	31.79 (15.27)	NA	NA	NA
60 min	1.30×10^6 (1.2×10^5)	1.28×10^4 (5.2×10^3)	5.26 (5.26)	NA	NA	NA

[a] The data out of the brackets show resistivity of the fibres (ρ_f) while that in the brackets represent resistivity of bare surface coatings (ρ_c).
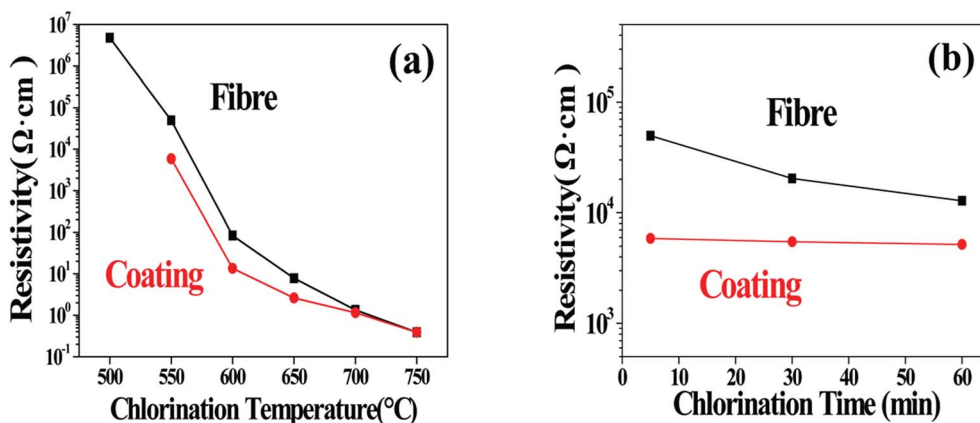

Fig. 8 (a) Resistivity of fibres chlorinated for 5 min at temperature range of 500–750 °C. (b) Resistivity of fibres chlorinated for 5, 30, 60 min at 550 °C.

fibre of 750-5 is still amorphous, the porous structure facilitates a totally different contrast in the TEM bright field image with more loosely packed nanophases (Fig. 7c). By enlarging this region, large amount of turbostratic carbon clusters can be observed (Fig. 7d). It should be noted that the free carbon in the C–SiC$_x$O$_y$ hybrid phases is actually present in two forms of CDC and PyC. The former is filled with micropores that generated during halogen etching, while the latter is dense since the pores induced by decomposition of the PCS fibre have already closed during the significant volume shrinkage in pyrolysis.[2] The content of PyC is unlikely to be changed by the current treatments since the chlorination temperatures are much lower than the decomposition point of SiC$_x$O$_y$. Therefore, the carbon clusters in Fig. 7d should be identified as CDC rather than PyC since they are invisible in the fibre before chlorination.

It is interesting to note that the reactivity of Cl$_2$ with sintered SiC particles of micro size[31] is identified to be much lower as compared with the current experiment. This is probably due to the fact the surface energy of the SiC nano grains in the fibre is much higher than that of the large SiC particles. Moreover, the polymer–ceramic conversion endows the SiC fibres with active sites (such as dangling bonds induced by cleavage of the Si–H) of much higher concentration than sintered SiC, which may also contribute to enhancing the reactivity of the fibre to the Cl$_2$.

Considering that the SiC$_x$O$_y$ phases behave as insulators while the free carbon is much more conductive,[32,33] the change of the C/SiC$_x$O$_y$ ratio in the coating should also be reflected by the evolution of the specific resistivity of the coated SiC fibres (ρ_f). The influence of the treating parameters on the ρ_f is listed

in Table 3 and also shown in Fig. 8. For soaking time of 5 min, ρ_f decreases steadily over 7 orders of magnitude (from 5.01×10^6 to 0.39 Ω cm) as the temperature increasing from 500 to 750 °C. According to conductor skin effects, the current may only go through the C–SiC$_x$O$_y$ coatings because of its much lower resistance compared with the unreacted fibre core,[3] especially as the carbon yield of the coating is enhanced. In consideration of this, the specific resistivity of the bare C–SiC$_x$O$_y$ coatings (ρ_c) is also calculated based on its hollow cylinder shape. With temperature increasing, ρ_c declines in a trend similar to ρ_f, and approaches ρ_f because of the increase in the coating thickness. The huge change in ρ_c should be induced by the change of C/SiC$_x$O$_y$ ratios through consumption of oxygen and formation of CDC. With the depletion of SiC$_3$O and SiC$_2$O$_2$ at above 750 °C, the resistivity of the C–SiC$_x$O$_y$ coating is close to that of the amorphous carbon,[34] indicating that the isolated carbon islands tend to connect as a conductive network. Fig. 8b shows that the isothermal process has ignorable influence on the coating resistivity, which is consisting with the AES/XPS results that the composition of C–SiC$_x$O$_y$ coating is almost independent of treating time.

In order to know the feasibility of the C–SiC$_x$O$_y$ coatings as interphase layers, two kinds of coated fibres (550-30 and 650-5) with approximate thickness are selected to fabricate SiC$_f$/SiOC ceramic composites. Fig. 9 shows the fracture surface of the SiC$_f$/SiOC composites reinforced with 550-30 fibre and 650-5 fibre respectively. Both composites show obvious interface debonding and fibre pullout. Length of the fibre pullout in the 650-5 composite is larger than that in the 550-30 composite,
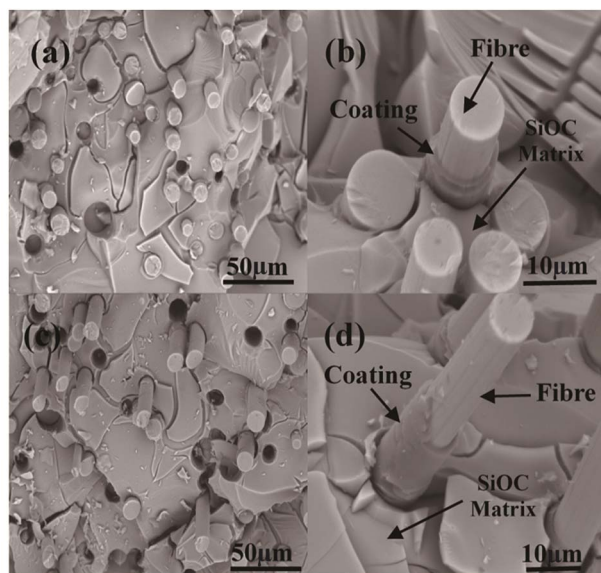
Fig. 9 Fracture surface of the SiC$_f$/SiOC ceramic composites. (a) SiC$_f$/SiOC reinforced with 500-30 fibres and (b) the enlarged image of a fractured fibre. (c) SiC$_f$/SiOC reinforced with 650-5 fibres and (d) the enlarged image of a fractured fibre.

suggesting that the bonding at the fibre/matrix interface is weakened as the formation temperature of the C–SiC$_x$O$_y$ coating is elevated and the CDC content of the coating is increased.

In general, the chlorination offers flexibility in adjusting the microstructure of the C–SiC$_x$O$_y$ coatings on oxygen-enriched SiC fibres. By adjusting the coating composition, interfacial debonding state of the ceramic composites can be changed and mechanical performance of the composite can be easily modified. Considering the great variability of resistivity, the coated SiC fibres may generate controllable dielectric losses in electromagnetic wave (EMW), which thus has potential for preparing advanced composites for stealth devices.

4 Conclusion

The current work focuses on preparation and characterization of C–SiC$_x$O$_y$ coatings formed on oxygen-enriched SiC fibres. The main conclusions are summarized as follows:

(1) Formation of the C–SiC$_x$O$_y$ coatings is identified to be a result of the select etching of the SiC$_x$O$_y$ metaphases by Cl$_2$. The chlorination temperature is a key factor to change the coating composition, while the soaking time is mainly related to variation of the coating thickness. Thus, the composition and the thickness of the coatings can be independently regulated to meet different purposes.

(2) SiOC ceramic composites reinforced with the coated fibres show obvious interface debonding and fibre pullout. The fibre pullout length in the 650-5 composite is larger than that in the 550-30 composite, suggesting that the bonding at the fibre/matrix interface is weakened as the increase of the CDC content in the C–SiC$_x$O$_y$ coating.

(3) Through changing the composition of the C–SiC$_x$O$_y$ coating, the resistivity of the coated SiC fibres changed over 7 orders of magnitude. Combing the superiorities of high strength retain ratio, the C–SiC$_x$O$_y$ coated SiC fibres are promising for the development of newly structural composites with electric and dielectric functions.

Conflicts of interest

We declare that we do not have any commercial or associative interest that represents a conflict of interest in connection with the work submitted.

Acknowledgements

References

1 S. Yajima, J. Hayashi and M. Omori, *Nature*, 1976, **261**, 683–685.

2 A. R. Bunsell and A. Piant, *J. Mater. Sci.*, 2006, **41**, 823–839.

3 T. Shikawa, *Compos. Sci. Technol.*, 1994, **51**, 135–144.

4 N. P. Bansal, *Mater. Today*, 2005, **8**, 57.

5 E. Buet, C. Sauder and S. Poissonnet, *J. Eur. Ceram. Soc.*, 2012, **32**, 547–557.

6 R. Naslain, *Compos. Sci. Technol.*, 2004, **64**, 155–170.

7 N. Carrère, E. Martin and J. Lamon, *Composites, Part A*, 2000, **31**, 1179–1190.

8 J. P. Singh, D. Singh and M. Sutaria, *Composites, Part A*, 1999, **30**, 445–450.

9 K. Shimoda, J. S. Park and T. Hinoki, *Compos. Sci. Technol.*, 2008, **68**, 98–105.

10 H. Araki, W. Yang, H. Suzuki and Q. Hu, *J. Nucl. Mater.*, 2004, **329**, 567–571.

11 S. Jacques, A. Lopez-Marure and C. Vincent, *J. Eur. Ceram. Soc.*, 2000, **20**, 1929–1938.

12 Y. G. Gogotsi and M. Yoshimura, *Nature*, 1994, **367**, 628–630.

13 L. Chen, G. Behlau and Y. Gogotsi, *Carbide derived carbon (CDC) coatings for Tyranno ZMI SiC Fibers*, John Wiley & Sons, 2003, vol. 4, pp. 57–62.

14 M. J. Yuan, T. Zhou and J. He, *Appl. Surf. Sci.*, 2016, **382**, 27–33.

15 L. Chen, H. Ye, Y. Gogotsi and M. J. McNallan, *J. Am. Ceram. Soc.*, 2003, **86**, 1830–1837.

16 L. Chen, H. Ye and Y. Gogotsi, *J. Am. Ceram. Soc.*, 2004, **87**, 147–151.

17 L. Shen, B. J. Tan, W. S. Willis, F. S. Galasso and S. L. Suib, *J. Am. Ceram. Soc.*, 1994, **77**, 1011–1016.

18 A. Delcamp, *et al.*, *Surf. Coat. Technol.*, 2010, **205**, 703–709.

19 G. Chollon, R. Pailler and R. Canet, *J. Eur. Ceram. Soc.*, 1998, **18**, 725–733.

20 A. Jänes, T. Thomberg and E. Lust, *Carbon*, 2007, **45**, 2717–2722.

21 S. H. Yeon, P. Reddington and Y. Gogotsi, *Carbon*, 2010, **48**, 201–210.

22 K. S. W. Sing, *Pure Appl. Chem.*, 1985, **57**, 603–619.

23 S. Yu, R. Tu and T. Goto, *J. Eur. Ceram. Soc.*, 2016, **36**, 403–409.

24 M. A. Rooke and P. M. A. Sherwood, *Carbon*, 1995, **33**, 375–380.

25 A. Avila, I. Montero and L. Galan, *J. Appl. Phys.*, 2001, **89**, 212–216.

26 B. Su, H. Liang and G. Liu, *J. Eur. Ceram. Soc.*, 2018, **38**, 2289–2296.

27 S. Stankovich, D. A. Dikin and R. D. Piner, *Carbon*, 2007, **45**, 1558–1565.

28 A. P. Dušan, J. Marschall and M. R. George, *J. Eur. Ceram. Soc.*, 2010, **30**, 2289–2300.

29 C. Laffon, A. M. Flank and P. Lagarde, *J. Mater. Sci.*, 1989, **24**, 1503–1512.

30 G. Honstein, C. Chatillon and F. Baillet, *J. Eur. Ceram. Soc.*, 2012, **32**, 1117–1135.

31 Y. G. Gogotsi, *J. Mater. Chem.*, 1997, **7**, 1841–1848.

32 M. S. Cao, W. L. Song and Z. L. Hou, *Carbon*, 2010, **48**, 788–796.

33 R. Bodet, N. Jia and R. E. Tressler, *J. Eur. Ceram. Soc.*, 1996, **16**, 653–664.

34 F. Carmona, P. Delhaes and G. Keryer, *Solid State Commun.*, 1974, **14**, 1183–1187.

This journal is © The Royal Society of Chemistry 2019